Title

ChemInform Abstract: Synthesis, Structure, Thermoelectric Properties, and Band Gaps of Alkali Metal Containing Type I Clathrates: A8Ga8Si38 (A: K, Rb, Cs) and K8Al8Si38.

Journal

ChemInform, 46(27)

ISSN

0931-7597

Authors

Sui, Fan
He, Hua
Bobev, Svilen
et al.

Publication Date

2015-07-01

DOI

10.1002/chin.201527010

CHEMISTRY OF MATERIALS

Article

pubs.acs.org/cm

Synthesis, Structure, Thermoelectric Properties, and Band Gaps of Alkali Metal Containing Type I Clathrates: $A_8Ga_8Si_{38}$ (A = K, Rb, Cs) and $K_8Al_8Si_{38}$

Fan Sui,[†] Hua He,[‡] Svilen Bobev,[‡] Jing Zhao,[†] Frank E. Osterloh,[†] and Susan M. Kauzlarich*,[†]

[†]Department of Chemistry, University of California, One Shields Avenue, Davis, California 95616, United States

[‡]Department of Chemistry and Biochemistry, University of Delaware, Newark, Delaware 19716, United States

Supporting Information

ABSTRACT: A series of alkali metal containing compounds with type I clathrate structure, $A_8Ga_8Si_{38}$ (A = K, Rb, Cs) and $K_8Al_8Si_{38}$, were synthesized and characterized. Room temperature lattice parameters of $A_8Ga_8Si_{38}$ (A = K, Rb, Cs) and $K_8Al_8Si_{38}$ were determined to be 10.424916(10), 10.470174(13), 10.535069(15), and 10.48071(2) Å, respectively. The type I clathrate structure (cubic, $Pm\bar{3}n$) was confirmed for all phases, and in the case of $K_8Al_8Si_{38}$ and $K_8Ga_8Si_{38}$, the structures were also refined using synchrotron powder diffraction data. The samples were consolidated by Spark Plasma Sintering (SPS) for thermoelectric property characterization. Electrical resistivity was measured by four probe AC transport method in the temperature range of 30 to 300 K. Seebeck measurements from 2 to 300 K were consistent with $K_8Al_8Si_{38}$ and $K_8Ga_8Si_{38}$ being n-type semiconductors, while $Rb_8Ga_8Si_{38}$ and $Cs_8Ga_8Si_{38}$ were p-type semiconductors. $K_8Al_8Si_{38}$ shows the lowest electrical resistivity and the highest Seebeck coefficient. This phase also showed the largest thermal conductivity at room temperature of ~1.77 W/Km. $K_8Ga_8Si_{38}$ provides the lowest thermal conductivity, below 0.5 W/Km, comparable to the type I clathrate with heavy elements such as $Ba_8Ga_{16}Ge_{30}$. Surface photovoltage spectroscopy on films shows that these compounds are semiconductors with band gaps in the range 1.14 to 1.40 eV.

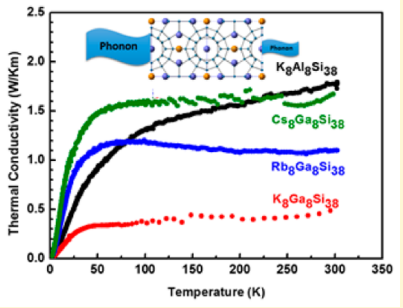

1. INTRODUCTION

Thermoelectric materials have been intensively studied over the past decades as they can recycle waste heat and therefore enhance energy use ratio. They can also generate cool air without discharge of greenhouse gases. Research has focused on improving the efficiency of thermoelectric materials, which is related to the figure of merit, zT. Slack proposed the phonon glass, electron crystal (PGEC) concept in 1994, i.e., materials with optimal thermoelectric performance should be semiconductors with glass-like thermal conductivity (κ) and crystal-like electrical conductivity (σ).[1] It is a significant challenge to achieve high Seebeck coefficient and electrical conductivity while keeping the thermal conductivity low, as these thermoelectric properties are interrelated; changing one property inevitably affects the others.

Inorganic clathrate compounds are characterized by an open framework structure with guest atoms trapped in well-crystallized host framework structure.[2,3] The rattling motion of the guest atoms can decrease thermal conductivity, while the highly ordered framework can guarantee the propagation of carriers. Therefore, inorganic clathrates, with their unique structure, are considered to be PGEC materials with potential for thermoelectric applications.[4−6] Type I clathrate structure, shown in Figure 1, is characterized by 20-vertex pentagonal dodecahedra and 24-vertex tetrakaidecahedra, comprised of tetrahedrally bonded framework atoms, which are mainly group 14, 15 atoms and can be substituted by group 13 atoms or transition metals.[7,8] Group 1, 2 atoms or a few halogens occupy 2*a* sites inside the 20 vertex cages and 6*d* sites in the 24 vertex cages, as guest atoms.

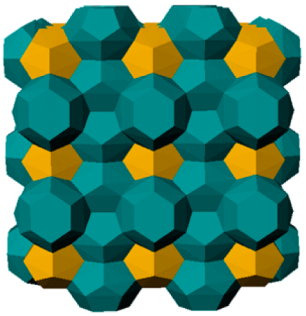

Figure 1. A view of the structure of Type I clathrate showing the two types of cages. The 20- and 24-vertex cages are shown in gold and green, respectively.

Silicon based type I clathrates have drawn intense research interest, since silicon is the second most abundant element in earth's crust, is environmentally friendly, and is stable in high

Received: December 2, 2014
Revised: March 24, 2015
Published: March 25, 2015

DOI: 10.1021/cm504436v
Chem. Mater. 2015, 27, 2812−2820

temperature range (up to 1687 K). These observations make silicon-based clathrate phases of interest for large-scale applications, both for thermoelectric applications and, more recently, as direct or nearly direct band gap semiconductors.[9,10] In addition, compared to Ge and Sn, which are also common elements in type I clathrates compounds, Si is a light element and therefore is advantageous for applications that involve transportation or where weight might be a limiting requirement. Therefore, Si-containing phases are promising candidates for thermoelectric devices that might be envisioned for automotive or aerial transportation. Many Si-based materials, such as SiGe alloys and Mg_2Si,[11,12] have achieved superior thermoelectric performance. They all have high power factors ($S^2\sigma$) but also fairly high thermal conductivities (2−6 W/Km). Research has focused on various approaches to decrease the thermal conductivity by introducing nanostructure or nanoparticles in the main phase.[13−15] The crystal structure of Si-based clathrates provides an alternative approach because the structure naturally allows for good electrical transport through the framework while keeping the thermal conductivity low with rattling guest atoms.[16]

$Ba_8Al_{16}Si_{30}$ with type I clathrate structure has been characterized with an aim toward potentially high thermoelectric efficiency at high temperatures.[17−19] The phase range, structure, and thermoelectric properties of $Ba_8Al_xSi_{46-x}$ type I clathrates have been previously investigated.[20−22] $Ba_8Al_{14}Si_{31}$ has a zT reaching 0.34 at 1150 K, and all the samples showed relatively low thermal conductivity (∼2 W/Km).[17] Further improvement can be achieved by optimizing the carrier concentration. The silicon framework is partially substituted by Al to compensate the electrons from ionization of Ba. However, in all of these phases, the amount of Al in $Ba_8Al_xSi_{46-x}$ never reaches the ideal value of 16 which should result in a semiconductor.[23]

The structure of type I Si clathrate $K_8Ga_8Si_{38}$ was reported,[24,25] and the electronic structure calculations indicated that this phase should have semiconducting transport properties.[25] The electronic properties were experimentally determined by optical and single crystal transport measurements to be consistent with a narrow band gap semiconductor. The compositions, $A_8Tr_8Si_{38}$ (A = K, Rb, Cs; Tr = Al, Ga), have been investigated using first-principles calculations, and the hole-doped $Cs_8Ga_8Si_{38}$ phase was proposed to have a high zT of ∼0.75.[26] Alkali metal-containing $K_8M_8Sn_{38}$ (M = Al, Ga, and In) compounds with the type I clathrate structure have been synthesized, and their thermoelectric properties were characterized yielding a maximum zT at 440 K of 0.25.[27,28] The single crystal structures of $K_8Al_8Si_{38}$, $K_8Ga_8Si_{38}$, and $Rb_8Ga_8Si_{38}$ have been reported.[9,24,29] The optical properties of $K_8Al_8Si_{38}$ indicate that it is a semiconductor with a quasi-direct gap of about 1.3 eV.[9] Theoretical calculations indicate the cage structural disorder introduced by aluminum substitution plays an important role in determining the thermal conductivity, in addition to the rattling motion of guest atoms.[30] Most recently, $A_8Al_8Si_{38}$ (A = K, Rb, Cs) phases have been reported, and magnetic and transport measurements as well as quantum chemical calculations were presented.[31] The Seebeck coefficient, along with electrical resistivity measurements, provided very high values interpreted via a variable range hopping model.

In this paper, we report the synthesis and characterization of the series of compounds, $A_8Ga_8Si_{38}$ (A = K, Rb, Cs) and $K_8Al_8Si_{38}$, and report their structure thermoelectric properties and band gap measurements. These compounds are made of all earth-abundant elements whose compositions should be close to ideal for semiconducting behavior. The possibilities of further chemical optimization make these compounds an important series to study for the application of energy conversion.

2. EXPERIMENTAL PROCEDURES

2.1. Materials. Elemental K, Rb, Cs, Ga, and Si, purchased either from Alfa Aesar or Aldrich with the stated purity above 99.5%, were used as starting materials. Potassium hydride (KH, Sigma-Aldrich, 30 wt % dispersion in mineral oil) was purified by washing with hexane in nitrogen filled glovebox to remove the mineral oil residue, and hexane was removed through evacuation. All manipulations involving alkali metals or KH were performed inside an argon-filled glovebox with O_2/H_2O level below 1 ppm or under vacuum due to their high reactivity to air and moistures. Al shot (99.999%, Furuchi Chem. Co., Japan) and Si lump (Alfa Aesar, 99.99999+%) were arc melted into an ingot and then pulverized in a tungsten carbide grinding vial with a SPEX 8000 M SamplePrep Mixer/Mill.

Caution: KH powder and K, Rb, and Cs metals are reactive to oxygen and moisture and must be handled with care under an inert atmosphere.

2.2. Synthesis. *$A_8Ga_8Si_{38}$ (A = K, Rb, Cs)* − Type I clathrates $A_8Ga_8Si_{38}$ (A = K, Rb, Cs) were synthesized via solid-state reactions at high temperature. For this purpose, the elements A, Ga, and Si in a molar ratio of 9:8:38 were loaded into niobium or tantalum tubes, where the 10% excess alkali metals were added to compensate for their volatility. The Nb/Ta tubes were arc welded under high purity argon and then jacketed in fused silica tubes, which were subsequently flame-sealed under vacuum. The reaction vessels were subjected to heat treatment at 700 °C for 6 days. The products thus obtained were usually chunks of polycrystalline samples. The crystal quality and phase purity was greatly improved by crushing these chunks of sample and annealing them at 700 °C for 3 days in Nb/Ta tubes sealed in the manner described above. The final samples obtained after anneal were soaked in 1.0 M NaOH solution to remove trace amounts of silicon and air-sensitive side products, e.g., K_2Ga_3, $CsGa_7$.

$K_8Al_8Si_{38}$ − Al metal shot and Si pieces were weighed in air, arc melted under an Ar atmosphere, crushed into smaller pieces, and transferred into a glovebox where the KH powder was weighed. The Al−Si and KH powders, in the molar ratio of 9:9:38 (KH: Al: Si), were put into a 5 mL tungsten carbide lined grinding vial with two tungsten carbide balls, sealed in an airtight aluminum coated plastic bag and mechanically ground with a SPEX Mixer/Mill for 30 min. The slight excess of KH and Al were required for phase pure product. The resulting gray powder was then transferred into a niobium ampule, which was sealed under argon atmosphere by an arc-welder. The Nb ampule was then sealed in a fused silica tube under vacuum and annealed at 950 °C for 10 h and 700 °C for 40 h in an electric box furnace. After annealing, the reaction vessel was furnace cooled and transferred to a glovebox where it was opened. The product was then removed from the glovebox, and any excess K or Al was removed by washing the sample with ethanol and diluted hydrochloric acid. It was determined that the clathrate phase is stable toward both ethanol and dilute hydrochloric acid. The product is a fine dark gray powder and characterized by powder XRD.

2.3. Single Crystal Diffraction. Crystallographic data of $A_8Ga_8Si_{38}$ (A = K, Rb, Cs) samples were collected on a Bruker SMART CCD-based diffractometer with Mo Kα radiation (λ = 0.71073 Å) at 200 K. The collected frames were integrated using the SAINT package. Analytical absorption correction was performed using SADABS. The structure solution was obtained by direct methods and refined by full-matrix least-squares refinement against F_0^2 using the SHELXTL package. The crystal structure of $K_8Al_8Si_{38}$ was reported in previous work.[9]

2.4. Powder X-ray Diffraction. $A_8Tr_8Si_{38}$ (A = K, Rb, Cs; Tr = Al, Ga) samples were ground into fine powder for powder X-ray diffraction (PXRD) analysis. A zero background quartz sample holder was used for room temperature data collection with a Bruker D8

DOI: 10.1021/cm504436v
Chem. Mater. 2015, 27, 2812−2820

Table 1. Comparison of Lattice Parameters Determined from Single Crystal X-ray Diffraction and Powder Diffraction[a]

parameter	comments			
compound	$K_8Al_8Si_{38}$	$K_8Ga_8Si_{38}$	$Rb_8Ga_8Si_{38}$	$Cs_8Ga_8Si_{38}$
lattice parameters (Å) from single crystal X-ray diffraction, temperature (K)		10.427(1), 293[24]		
	10.4802(16), 90[9]	10.4261(2), 293[25]	10.469(2), 293[29]	10.5339(3), 200
	10.470(1), 293[31]	10.4270(3), 200	10.4433(15), 200	
lattice parameters (Å) from powder X-ray diffraction	10.4886(6)[31]	10.424916(10)	10.470174(13)	10.535069(15)
	10.48071(2)			
Ga occupancy at 24*k* site		17.5%[24]		
		17.9(2)%[25]	22.0%[29]	20.2(3)%
		17.7(4)%	17.8(4)%	
Ga occupancy at 16*i* site		1.9%[24]		
		2.59(19)%[25]	1.2%[29]	1.07(3)%
		3.2(3)%	0.4(4)%	
Ga occupancy at 6*c* site		56.6(2)%[24]		
		60.7(5)%[25]	40.9(5)%[29]	46.2(5)%
		61.0(7)%	52.0(9)%	

[a]Ga occupancies at the framework sites determined from single crystal X-ray diffraction.

Advance diffractometer operated at 40 kV and 40 mA utilizing Cu *Kα* radiation. Unit cell refinement was performed with FullProf Suite.[32]

2.5. Synchrotron X-ray Diffraction. $K_8Al_8Si_{38}$ and $K_8Ga_8Si_{38}$ samples were sent to the Advance Photon Source at the U.S. Department of Energy's Argonne National Laboratory. Data collection was performed at 11-BM with radiation wavelength of 0.469659 Å. Since the samples have relatively low atomic number and weak scattering, Cole-Parmer Kapton tubes with the inner diameter of 0.0575″ (1.46 mm) were used to enhance the data intensity. The powder samples were transferred into the Kapton tubes, sealed with clay, and inserted vertically into the sample base. Rietveld refinement was performed with JANA 2006 package.

2.6. Electron Microprobe Characterization. Sintered pellets after thermoelectric characterization were used for electron microprobe X-ray diffraction measurements. The pellets were mounted in epoxy and polished for analysis on a Cameca SX-100 electron microprobe equipped with five wavelength-dispersive spectrometers. The chemical compositions have been determined by wavelength-dispersive X-ray spectroscopy (WDXS) using the intensities of the characteristic X-ray lines. The following X-ray emission lines and standards were employed: K*α* lines of K from orthoclase standard, Al from aluminum standard, Si from silicon single crystal standard, and L*α* of Ga from GaAs standard, Cs from CsCl standard, and Rb from $RbTiO(PO_4)$. The determined chemical compositions are calculated from the atomic weight percentage of 10 points from each sample, with the total weight percent of 100 ± 0.8% to ensure the accuracy.

2.7. Thermoelectric Properties Sample Preparation. The $K_8Al_8Si_{38}$ sample was consolidated into a 4 mm diameter cylinder by a SPSS (Spark Plasma Sintering System) at 650 °C and 5 kN. The $A_8Ga_8Si_{38}$ (A = K, Rb, Cs) samples were consolidated at 600 °C and 5 kN. Geometric densities of 86−89% were achieved. The sintered cylinder shaped samples were cut into about 1 mm thick pellet with a diamond saw.

2.8. Room Temperature Thermoelectric Properties Measurement. The thermoelectric properties were measured (2 K ∼ 300 K) with a PPMS (Physical Property Measurement System) thermal transport option and AC transport option. For the thermal transport option (TTO) 2 point method, the 4 mm cylinder is sliced into a pellet, about 1 mm in thickness and attached in between lead disc with silver conductive epoxy. The sample with leads then was dried in vacuum oven at 150 °C for 2 h to allow for good conductance of the epoxy. For four probe measurement in the AC transport option, the sample was placed on the sample puck and connected to the four electrodes (I^+, I^-, V^+, V^-) with platinum wire, attached by acetone based silver paste.

2.9. Surface Photovoltage Spectroscopy. Samples for surface photovoltage measurements were prepared on conductive Au-coated glass slides (Thermo Scientific BioGold Microarray Slides, 12-550-59) of 1 × 1 cm^2, which were precleaned by first rinsing with acetone and then soaking in 30% H_2O_2 aqueous solution containing 0.05 M KOH, followed by a final thorough rinse with Milli-Q pure water and drying in air. Powders of materials for testing were suspended in ethanol and drop-cast onto the Au substrates and then left in air for drying off the solvent. Signals of Contact Potential Difference (CPD) were recorded in vacuum (10^{-7} bar) using a vibrating gold mesh reference probe (Kelvin Probe, 3 mm in diameter, *Delta PHI Besocke*) and a Kelvin control 07 (*Delta PHI Besocke*) with a sensitivity of 1 mV. Sample-probe distance was kept constant at ca. 1 mm. A 175 W Xe arc lamp (PE175-BF) was used as the light source, in conjunction with a monochromator (Cornerstone 130 with 600−2500 nm Newport grating 74028) to provide monochromatic illumination with an average peak fwhm of 30 nm. Photovoltage spectra were collected and corrected for drift effects due to pressure variations by subtracting a linear background signal drift.

3. RESULTS AND DISCUSSION

3.1. Synthesis. Pure phase compounds $A_8Ga_8Si_{38}$ (A = K, Rb, Cs) were synthesized by the combination of the elements with approximately 10% excess alkali metals in sealed Nb/Ta tubes. When this method was employed for $K_8Al_8Si_{38}$, a small number of single crystals were obtained and the structure solution reported;[9] however, the majority of the sample was a mixture of $K_8Al_8Si_{38}$ and Si predominately. Systematic investigation of various heating profiles and composition for the Al-containing compound suggested that the poor solubility of K in Al or Si inhibits the formation of a high-yield product. The use of KH and Al−Si powder as starting reagents and ball milling the powders combined with higher annealing temperature proved to be successful in preparing phase-pure product. Approximately a 10% excess of both KH and Al was necessary to achieve a phase-pure powder diffraction pattern of type I clathrate. It is possible that the Al reacts with the hydrogen byproduct of KH to give AlH_3 which then results in a deficiency of Al in the clathrate structure, so the relative stoichiometry of KH:Al:Si of 9:9:38 provided the best sample. The amount of Al was investigated by employing various Al_xSi_{46-x} starting powders with excess KH according to the ratio of $9{:}x{:}38 - x$. For $x < 9$, Si was present in the powder diffraction patterns, and for $x \geq 9$ the lattice parameter reached a constant value of ∼10.48 Å (see SFigure 1 in the Supporting Information). Recently, the $A_8Al_8Si_{38}$ (A = K, Rb, Cs) series was prepared from a

DOI: 10.1021/cm504436v
Chem. Mater. 2015, 27, 2812−2820

combined metal−metal halide flux, providing an alternative route to these heavier alkali metal-containing phases.[31]

3.2. Structures and Chemical Composition. Single crystal X-ray diffraction at 200 K shows that the $A_8Ga_8Si_{38}$ (A = K, Rb, Cs) samples are isostructural and crystallize in cubic space group $Pm\bar{3}n$ (No. 223). The structure of $K_8Al_8Si_{38}$ was previously studied by single crystal X-ray diffraction and confirmed to also crystallize in type I clathrate structure.[9] Details of the structure data collection and refinement parameters are given in STable 1 (see the Supporting Information). The $K_8Ga_8Si_{38}$ and $Rb_8Ga_8Si_{38}$ structures have been previously studied by single crystal X-ray diffraction at 293 K showing consistent results with our refinements (Table 1).[24,29,25] Similar to the previous studies, no vacancies in the guest atom sites were found in the crystal refinement process, and, therefore, site occupancies were set to be fully occupied.

The framework structures for $A_8Tr_8Si_{38}$ (Tr = group 13 element) are constructed of the bonding between three different atomic sites referred to by their Wyckoff symbol as 24*k*, 16*i*, and 6*c*. Figure 2 shows both cages with the framework

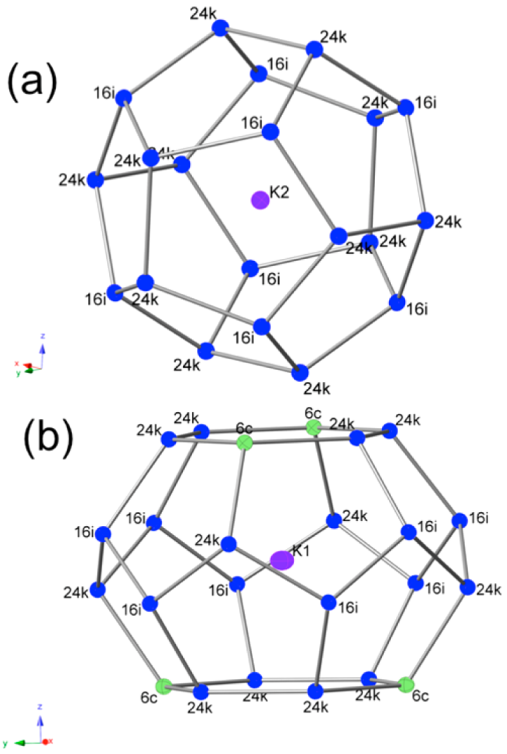

Figure 2. (a) E_{20}: 20 vertex dodecahedron cage (small) and (b) E_{24}: 24 vertex tetrakaidecahedron cage (large) of $K_8Ga_8Si_{38}$ with Wyckoff sites indicated. Thermal ellipsoid images of guest atoms are shown (75% probability).

labeled. The mixed occupancy sites of $A_8Ga_8Si_{38}$ were refined, and final Ga occupancies at the corresponding framework sites are listed in Table 1. The results indicate that Ga is not distributed evenly over the three sites. The site occupancy preference of gallium atoms affect the electronic property and band structure significantly.[33] Ga prefers to substitute the 6*c* and then the 24*k* sites but not the 16*i* site. The substitution preference for the 6*c* site is consistent with the occupancy rule of group 13 elements; that is, group 13 atoms prefer occupancies that can avoid direct chemical bond between group 13 elements.[34] However, the second preferred site of $A_8Ga_8Si_{38}$ (A = K, Rb, Cs) is 24*k* not 16*i*. This does not follow the preferred occupancy trend of $AE_8Tr_{16}Tt_{30}$ (AE = Ba, Sr; Tr = group 13; Tt = group 14) of 6*c* > 16*i* > 24*k* because as the framework for $A_8Tr_8Si_{38}$ has only 8 Ga atoms per unit cell, it is easier to avoid the Ga−Ga bond than in the case of $AE_8Tr_{16}Tt_{30}$. The 6*c* > 24*k* > 16*i* trend is consistent with the site occupancy preference reported for compound $Ba_8Al_xSi_{46-x}$ (x = 8).[20]

The unit cell parameters for $A_8Ga_8Si_{38}$ (A = K, Rb, Cs) determined from X-ray crystallography refinements increase with increasing guest atom size as expected (Table 1). The E_{20} and E_{24} cage volumes are plotted in Figure 3. The cage volumes

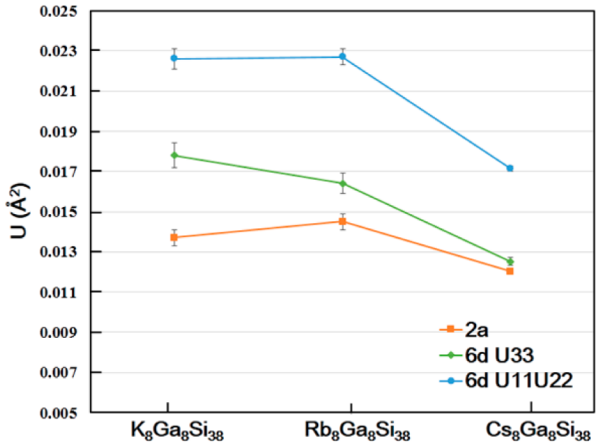

Figure 3. Atomic displacement of guest atom sites 2*a* and 6*d* U_{33} and $U_{11}(U_{22})$ of $K_8Ga_8Si_{38}$, $Rb_8Ga_8Si_{38}$, and $Cs_8Ga_8Si_{38}$ compounds. The anisotropic atomic displacement parameters of 6*d* site are plotted separately.

increase gradually as the guest atom gets larger, as the bond angles and lengths of the cages change to accommodate the guest atom. $K_8Al_8Si_{38}$ possesses a larger unit cell parameter compared with $K_8Ga_8Si_{38}$ regardless of temperature, though the covalent radius of Al (1.21 Å) is slightly smaller than that of Ga (1.22 Å).[35] This result is consistent with what has been observed for the series; in the case of $A_8Al_8Si_{38}$ all of the Al analogs have larger unit cells than the corresponding Ga phases.[31]

Figure 3 shows the atomic displacement parameters (ADPs) for the guest atoms which are identified by their Wyckoff symmetry as 2*a* (K2 in Figure 2) and 6*d* (K1 in Figure 2). The guest atom (2*a*) corresponding to the guest within the E_{20} cage show smaller ADP values with $U_{11} = U_{22} = U_{33}$ (Figure 3). The guest atom (6*d*) which is situated in the center of the E_{24} (24 vertex) cage possesses a large anisotropic ADP with $U_{11} = U_{22} > U_{33}$, and there was no additional residual electron density associated with this position, indicating that a split site might be a better model. The ADPs are equivalent at the directions parallel to the six-membered ring, and displacement at the direction perpendicular to the six-membered ring is smaller. This is also seen in the $Ba_8Al_{14}Si_{31}$ and $Ba_8Ga_{16}Si_{30}$.[36,37] The relative ratio between guest atom size (calculated from the ionic radius of guest atoms) and cage volume (Figure 4) can be calculated: Rb compound (9.33%) is slightly larger than K (7.00%), and Cs (12.09%) is the largest of the three. U_{33} ADPs at the direction normal to the hexagonal plane decrease as the relative ratios of guest atoms increase. The exception is the U_{11} and U_{22} directions of K and Rb atoms, which are about the

DOI: 10.1021/cm504436v
Chem. Mater. 2015, 27, 2812−2820

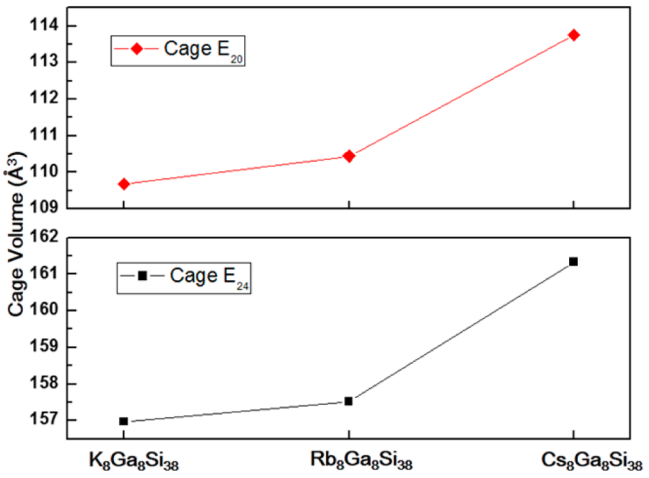

Figure 4. E_{20} and E_{24} cage volume (Å^3) for $A_8Ga_8Si_{38}$ (A = K, Rb, Cs).

same. The relative cage sizes influence the dynamic disorder of guest atoms to a great extent.[38] This dynamic disorder of guest atom in the E_{24} cage of type I clathrate can contribute to the decrease lattice thermal conductivity.[1,3]

Regardless of the temperature, the unit cell parameter of $K_8Al_8Si_{38}$ is larger than the Ga containing analog. The bond lengths of $K_8Al_8Si_{38}$ and $K_8Ga_8Si_{38}$ obtained from the refinement of single crystal X-ray diffraction data are listed in Table 2. The framework bonds of 24*k*−6*c* and 16*i*−16*i* bonds

Table 2. Bond Lengths (Å) of the Framework for $K_8Al_8Si_{38}$ and $K_8Ga_8Si_{38}$ Determined from Single Crystal X-ray Diffraction

	$K_8Al_8Si_{38}$ Bond Length (Å)[9]		
	24*k*	16*i*	6*c*
24*k*	2.450		2.488
16*i*	2.406	2.385	
	$K_8Ga_8Si_{38}$ Bond Length (Å)		
	24*k*	16*i*	6*c*
24*k*	2.460		2.449
16*i*	2.404	2.369	

are longer for $K_8Al_8Si_{38}$ than those of $K_8Ga_8Si_{38}$, while the 24*k*−24*k* bonds are shorter, and 24*k*−16*i* bonds do not have significant difference in lengths. These differences support the hypothesis that Al prefers to occupy the 6*c* and 24*k* sites with only a small amount of Al on the 16*i* site.[9] The largest difference of bond angles are at the hexagonal face of E_{24}, where the 24*k*−6*c*−24*k* angle of $K_8Al_8Si_{38}$ (111.786°) is slightly larger than $K_8Ga_8Si_{38}$ (111.606°), and the 6*c*−24*k*−24*k* angle of $K_8Al_8Si_{38}$ (124.107°) is slightly smaller than $K_8Ga_8Si_{38}$ (124.197°). As shown in Figure 2, E_{20} cage in type I clathrate is composed of 24*k*−24*k* and 24*k*−16*i* bonds, and the E_{24} cage is composed of 24*k*−6*c*, 16*i*−16*i*, and 24*k*−16*i*. Therefore, the 20 vertex $K_8Al_8Si_{38}$ cage volume of 109.20 Å^3 is slightly smaller than that of $K_8Ga_8Si_{38}$ (109.68 Å^3). As all the bonds of E_{24} cages in $K_8Al_8Si_{38}$ are longer than those in $K_8Ga_8Si_{38}$, the cage volume is larger (Al, 159.78 Å^3 vs Ga, 156.97 Å^3). Overall, as a result, $K_8Al_8Si_{38}$ has a larger unit cell parameter than $K_8Ga_8Si_{38}$. The slightly longer bond lengths and larger angles observed for $K_8Al_8Si_{38}$ may be a result of slight structural disorder of those sites as Al is more electropositive than Ga and therefore will have a more significant tendency to avoid any direct Al−Al interactions. Al may also interact more strongly with the K cations than Ga.[30]

3.3. Powder X-ray diffraction characterization. The purity of the powder samples was determined by powder X-ray diffraction at room temperature. The results of the calculated Bragg positions and whole pattern fitting (shown in SFigure 2 in the Supporting Information) indicate the four samples are phase-pure with type I clathrate structure with no secondary phases detected. The unit cell parameters of $A_8Ga_8Si_{38}$ (A = K, Rb, Cs), provided in Table 1, increase gradually as the ionic radius of guest atoms increases. The lattice parameters determined from powder XRD and single crystal XRD agree well except for the case of $Rb_8Ga_8Si_{38}$. This suggests that the $Rb_8Ga_8Si_{38}$ powder sample has a different stoichiometry than the single crystal $Rb_8Ga_xSi_{46-x}$. The lattice parameters of $K_8Al_8Si_{38}$ are larger than that of $K_8Ga_8Si_{38}$, consistent with what has recently been reported.[31,9]

$K_8Al_8Si_{38}$ and $K_8Ga_8Si_{38}$ were additionally characterized via synchrotron powder X-ray diffraction. The X-ray wavelength of the synchrotron beamline was 0.46966 Å; therefore the X-ray diffraction data, with $(\sin\theta)/\lambda > 1$, provide high reliability in detailed atomic structure and mixed occupancies refinement. The Rietveld refinements of $K_8Al_8Si_{38}$ and $K_8Ga_8Si_{38}$ X-ray diffraction patterns are shown in Figure 5. The refinement model matches the reflection data well with R_p = 0.0865 and 0.0631 for $K_8Al_8Si_{38}$ and $K_8Ga_8Si_{38}$, respectively. In the structure solution process of $K_8Al_8Si_{38}$, the lowest *R* factor can be obtained by assigning Al at the 6*c* site only, supporting the hypothesis that Al atoms prefer to occupy the 6*c* site first. The refinement of $K_8Ga_8Si_{38}$ gave the chemical formula of $K_8Ga_{7.9}Si_{38.1}$. The lattice parameters and Al site preference for $K_8Al_8Si_{38}$ are similar to that recently reported from neutron diffraction.[31] With a larger unit cell, the K guest atom on the 6*d* site of $K_8Al_8Si_{38}$ possesses slightly larger ADP (0.0307 Å^2) along the six-membered ring direction than that of $K_8Ga_8Si_{38}$ (0.0275 Å^2), but smaller ADP for the direction vertical to the six-membered ring, due to the difference in bond angles and bond lengths, as described above.

3.4. Chemical Composition. Electron microprobe analysis was performed on the cross section of sintered pellets prepared by SPS. The samples were sintered at 650 °C to avoid the sample decomposition, and the densities of sintered samples were all around 89%. A back scattered image showed the $A_8Ga_8Si_{38}$ (A = K, Rb, Cs) and $K_8Al_8Si_{38}$ main phase (SFigure 2, in the Supporting Information). The particle size of the $K_8Al_8Si_{38}$ phase is significantly smaller than the $A_8Ga_8Si_{38}$ phases which all show at least one large grain with grain boundaries. Energy dispersive spectroscopy (EDS) confirmed the presence of silicon and gallium silicon alloy side phases. WDSA (Wavelength Dispersive Spectroscopy Analysis) was performed on the surface of the sintered pellet to determine the chemical composition. The chemical composition of the four samples were determined by requiring the atom total to be 54: $K_{7.87(4)}Ga_{7.87(8)}Si_{38.24(7)}$, $Rb_{7.82(8)}Ga_{7.74(9)}Si_{38.43(17)}$, $Cs_{8.02(2)}Ga_{7.82(3)}Si_{38.16(4)}$, and $K_{7.90(6)}Al_{8.07(8)}Si_{38.03(6)}$. The chemical compositions determined from WDS are in good agreement with the refined chemical composition from X-ray crystallography with the exception of the $Rb_8Ga_8Si_{38}$ sample which contained a smaller amount of Ga ($Rb_8Ga_{7.50}Si_{38.50}$), as mentioned above.

3.5. Thermoelectric Properties. Studies of thermoelectric properties were carried out on the sintered 4 mm diameter dense pellets. The geometry densities of sintered samples are

DOI: 10.1021/cm504436v
Chem. Mater. 2015, 27, 2812−2820

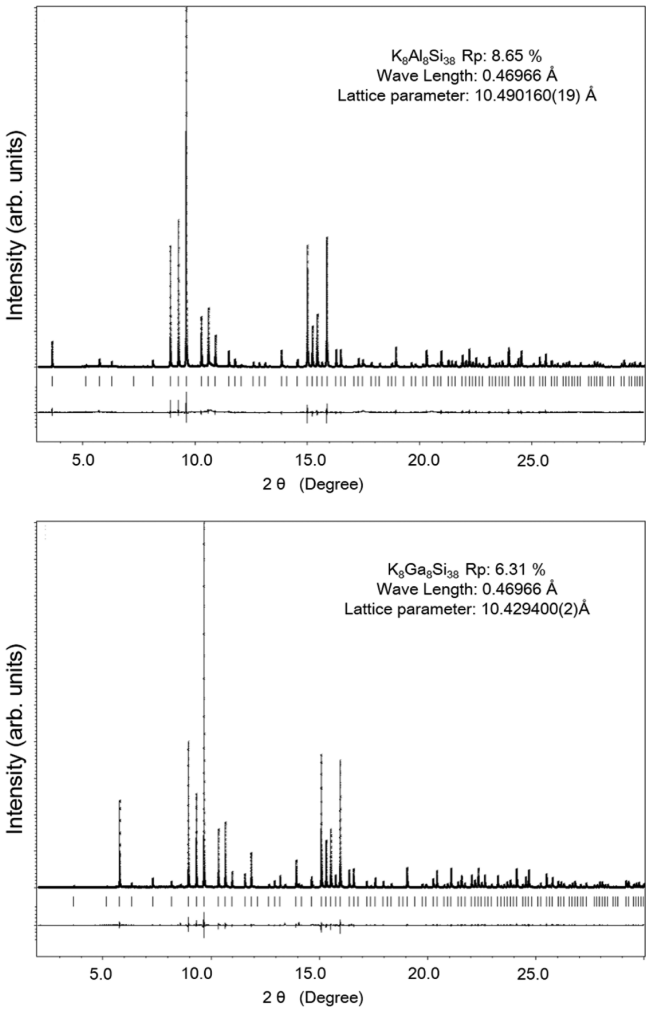

Figure 5. Rietveld refinement of synchrotron powder X-ray diffraction of $K_8Al_8Si_{38}$ and $K_8Ga_8Si_{38}$. The data are shown as dots, the calculated refinement as a line, the expected diffraction positions as tick marks, and the difference is indicated below the tick marks. The refinement *R* factors for $K_8Al_8Si_{38}$ are 8.65% (R_p) and 12.59% (wR_p). The refinement *R* factors for $K_8Ga_8Si_{38}$ are 6.31% (R_p) and 9.41% (wR_p).

89.19% ($K_8Ga_8Si_{38}$), 89.22% ($Rb_8Ga_8Si_{38}$), 86.35% ($Cs_8Ga_8Si_{38}$), and 86.25% ($K_8Al_8Si_{38}$). Figure 6 shows the temperature dependence (2 to 300 K) of the samples' total thermal conductivity (κ). The total thermal conductivities are the sum of κ_e, heat transferred by charge carriers, and κ_L, heat transferred by lattice vibration. κ_e can be calculated from the Wiedemann–Franz relation: $\kappa_e = L\sigma T$, where L is the Lorenz number, σ is the electrical conductivity, and T is temperature. The electrical resistivity of $A_8Ga_8Si_{38}$ is quite high; therefore, based on the Wiedemann–Franz relation, $\kappa_e \ll \kappa$, the charge carrier contribution to the total thermal conductivity is inconsequential.

The four samples show low thermal conductivity (below 2 W/Km) attributed to the clathrate complex structure, i.e., rattling guest atom and framework alloy scattering. Thermal conductivity values of $A_8Ga_8Si_{38}$ (A = K, Rb, Cs) increase from 2 K gradually and reach a plateau after 50 K. The thermal conductivity of $K_8Ga_8Si_{38}$ stays below 0.5 W/Km, which is comparable to the type I clathrate compounds with heavy elements, such as $Ba_8Ga_{16}Ge_{30}$.[39] $Rb_8Ga_8Si_{38}$ (~1.1 W/Km) and $Cs_8Ga_8Si_{38}$ (~1.6 W/Km), with the larger guest atom radius, showed higher thermal conductivity in this temperature range. The anisotropic dynamic disorder of guest atom, indicated by the large ADP of K1 (*6d* site) from single crystal X-ray diffraction, plays a critical role in the phonon transport. For the Ga–Si framework, the series of K, Rb, and Cs show the trend of lower κ with larger dynamic disorder of guest atom at *6d* site. When comparing $K_8Tr_8Si_{38}$ (Tr = Al, Ga), however, it is not the only factor that decides κ. The Ga–Si framework shows stronger alloy scattering because of the larger mass difference of Ga and Si, and this results in lower κ of $K_8Ga_8Si_{38}$ than $K_8Al_8Si_{38}$. Although $K_8Al_8Si_{38}$ shows the highest thermal conductivity compared with the Ga analog, it has lower thermal conductivity compared with the all Si-containing clathrate, K_8Si_{46}.[30] $K_8Al_8Si_{38}$ synthesized from Al and halides flux reaction has been reported and thermoelectric properties measured.[31] The thermal conductivity reported here (1.77 W/Km) is similar to their result on samples reported to be 96% dense (1.65 W/Km).[31]

Seebeck coefficients were measured simultaneously with thermal conductivity measurements (Figure 7). The absolute values of Seebeck coefficients increase linearly with increasing temperature; this suggests that the band structure can be approximated using a single parabolic band model. The negative Seebeck coefficient values of compounds $K_8Al_8Si_{38}$ and $K_8Ga_8Si_{38}$ indicate that electrons are the main carrier, while

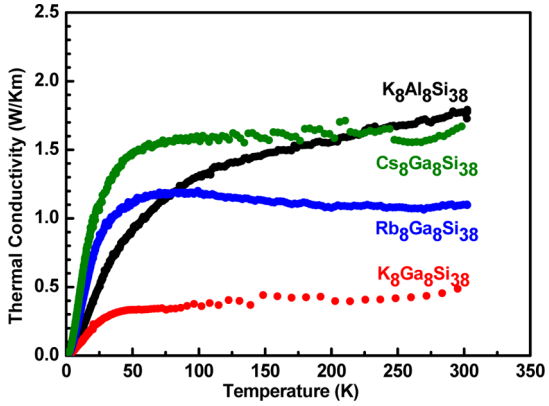

Figure 6. Thermal conductivity measurements of $A_8Ga_8Si_{38}$ (A = K, Rb, Cs) and $K_8Al_8Si_{38}$ SPSed pellets by PPMS thermal transport option.

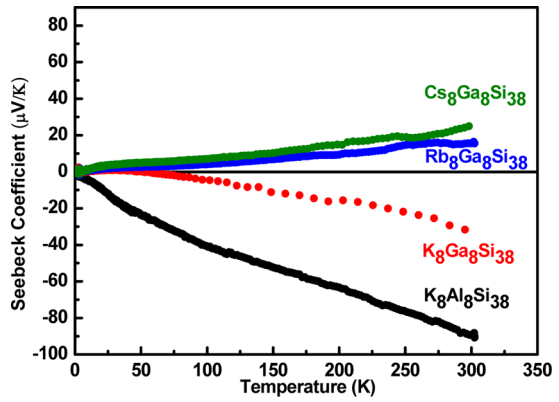

Figure 7. Seebeck coefficient measurement results of $A_8Ga_8Si_{38}$ (A = K, Rb, Cs) and $K_8Al_8Si_{38}$ SPSed pellets by PPMS thermal transport option.

DOI: 10.1021/cm504436v
Chem. Mater. 2015, 27, 2812–2820

the positive Seebeck coefficient values of compounds $Rb_8Ga_8Si_{38}$ and $Cs_8Ga_8Si_{38}$ indicate that holes are the main carrier. With similar framework structure, the carrier type experiences a transition from n-type to p-type when the guest atom type changes from K to Rb or Cs. $A_8Tr_8Si_{38}$ samples are electron balanced type I clathrate phases, as the A and Tr amount are equivalent. The alkali metal elements are electron donors, and the group 13 elements substitution in the Si framework can accept one electron each. A small deviation of A and Tr's relative ratio often decides the carrier types but is not the only reason.[40] Structure defects and the interaction between guest atoms and framework influence the carrier types as well.[40] Compared with all samples measured, $K_8Al_8Si_{38}$ shows the largest absolute Seebeck coefficient value at room temperature (~90 μV/K), significantly smaller than that recently reported (~200 μV/K).[31] This difference may be attributed to differences in the grain boundaries, phase purity, and composition of the pressed pellets.

The electrical resistivity data of the four samples from four-probe resistivity measurements are shown in Figure 8. The

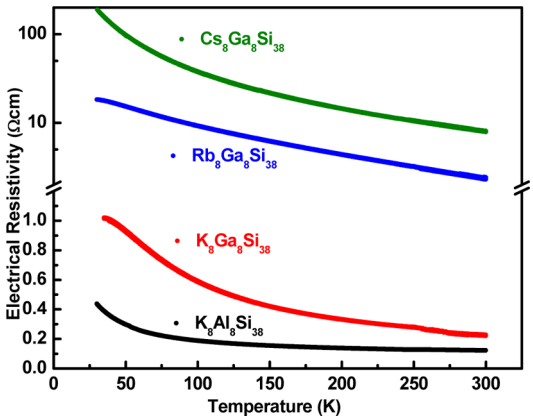

Figure 8. Electrical resistivity measurement results of $A_8Ga_8Si_{38}$ (A = K, Rb, Cs) and $K_8Al_8Si_{38}$ SPSed pellets by PPMS AC transport option.

samples all show semiconducting behavior as electrical resistivity decreases rapidly as the temperature increases from 30 to 300 K. However, they show high electrical resistivity values, which is disadvantageous to the thermoelectric performance. For example, $K_8Al_8Si_{38}$ has the lowest electrical resistivity among the four but still is more than 200 times higher than that of $Ba_8Ga_{16}Ge_{30}$.[41] From the microprobe analysis, the grain boundaries of the sintered samples may contribute to the high electrical resistivity (Supporting Information). The high resistivity is disadvantageous for the thermoelectric application, and further optimization of electrical conductivity by increasing carrier concentration through doping is necessary to enhance the thermoelectric properties. The electrical resistivities of $K_8Al_8Si_{38}$ and $K_8Ga_8Si_{38}$ were characterized previously and are in the same range of data provided herein.[25,31]

The carrier concentration (1.31×10^{18} cm^{-3}) and carrier mobility (~39 cm^2/(V s)) of $K_8Al_8Si_{38}$ were reported in an earlier study.[9] The carrier concentration of $K_8Ga_8Si_{38}$ is determined to be 3.12×10^{17} cm^{-3} from five-probe Hall measurement at 273 K, lower than that of $K_8Al_8Si_{38}$. The Seebeck coefficient follows the Pisarenko relation

$$\alpha = \frac{8\pi^2 k_B^2}{3eh^2} m^* T \left(\frac{\pi}{3n}\right)^{2/3}$$

where n is carrier concentration, and m^* is the carrier effective mass. Based on the measured carrier concentrations and Seebeck coefficients of $K_8Al_8Si_{38}$ and $K_8Ga_8Si_{38}$ at 273 K, their carrier effective mass can be calculated from the Pisarenko relation. $K_8Al_8Si_{38}$ has an effective mass about 8.33 times larger than that of $K_8Ga_8Si_{38}$, and this leads to a higher absolute Seebeck coefficient value of $K_8Al_8Si_{38}$. The absolute Seebeck coefficient values vs carrier concentrations of $K_8Al_8Si_{38}$ and $K_8Ga_8Si_{38}$ at 273 K were plotted in Figure 9 along with those

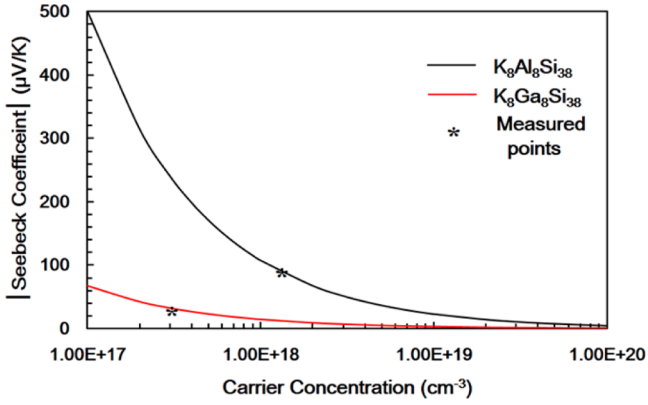

Figure 9. Pisarenko plots of $K_8Al_8Si_{38}$ (black line) and $K_8Ga_8Si_{38}$ (red line). The measured points at 273 K are shown in * and carrier concentration are plotted in logarithmic scale.

calculated from the Pisarenko relation. This plot suggests that if carrier concentration could be tuned the Seebeck coefficient for $K_8Al_8Si_{38}$ should be more sensitive because of the larger carrier effective mass.

The mobility of $K_8Ga_8Si_{38}$ is determined from the equation: $\sigma = n\mu e$, which is 82.03 cm^2/(V s). Compared to the mobility of $Ba_8Al_{15}Si_{31}$ (7.4 cm^2/(V s)) and $Ba_8Ga_{16}Si_{30}$ (8.4 cm^2/(V s)), $K_8Al_8Si_{38}$ and $K_8Ga_8Si_{38}$ compounds show high mobility values, which is beneficial to the thermoelectric performance.[19,42] The high mobility values indicate that substitutions in the framework of $A_8Tr_8Si_{38}$, which are much less than in the compounds of $AE_8Tr_{16}Si_{30}$ (AE = alkaline earth), do not negatively affect charge carrier transport while scattering phonon transport. $K_8Al_8Si_{38}$ and $K_8Ga_8Si_{38}$ are lightly doped semiconductors with low carrier concentration. Increasing carrier concentration by doping will enhance the electrical conductivity to a great extent.

3.5. Band Gap. Surface photovoltage (SPV) spectroscopy is a nondestructive and sensitive technique to probe light-induced charge separation and band gaps in molecular and bulk materials.[43−51] For the measurement, the contact potential difference of an illuminated sample film is recorded with a Kelvin probe as a function of the excitation energy. SPV spectra for $A_8Tr_8Si_{38}$ (A = K, Rb, Cs; Tr = Al, Ga) are shown in Figure 10. In all cases, a single negative photovoltage signal is observed above a characteristic onset energy, which can be taken as the band gap of each material. The absence of additional photovoltage features below the band gap suggests that these materials are free of midgap defects. As shown, $Cs_8Ga_8Si_{38}$ has the smallest band gap (1.14 eV), followed by $K_8Ga_8Si_{38}$ and $Rb_8Ga_8Si_{38}$ (both 1.18 eV). $K_8Al_8Si_{38}$ has the largest band gap value (1.40 eV) among this series, close to the literature value of 1.33 eV for $K_8Al_8Si_{38}$, as determined by optical absorption spectroscopy.[9] The similarity of the values (1.14 and 1.18 eV) for $A_8Tr_8Si_{38}$ with A = K, Rb, Cs agrees well with first-principle

DOI: 10.1021/cm504436v
Chem. Mater. 2015, 27, 2812−2820

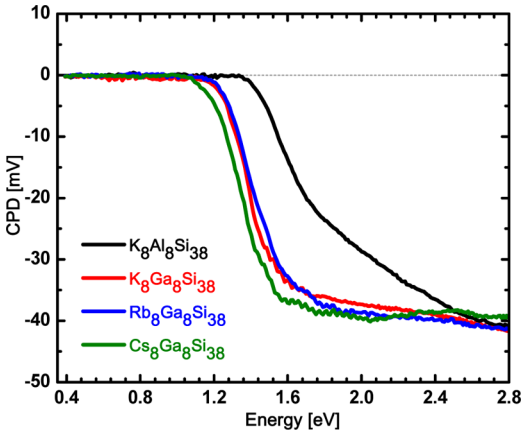

Figure 10. SPV spectra of $K_8Ga_8Si_{38}$ (red), $Rb_8Ga_8Si_{38}$ (blue), $Cs_8Ga_8Si_{38}$ (green), and $K_8Al_8Si_{38}$ (black) particle films on gold substrates. The contact potential difference (CPD) signal is plotted as a function of the illumination photon energy.

calculations by Nakamura et al. for the $A_8Ga_8Si_{38}$ (A = K, Rb, Cs) compounds.[26] According to this work the impact of guest atoms on the band gap should be minimal. The effect of the framework cations on the electronic structure is much stronger,[26] which explains the observed narrowing of the band gap (1.40 to 1.18 eV) (see Table 3) upon replacing Al with Ga atoms. Based on the negative sign of the photovoltage, all compounds behave as n-type semiconductors. This is in contrast with the Seebeck measurements described above. The discrepancy may be due to the different processing conditions for the samples (powdered films for SPV and spark-plasma sintered pellets for the Seebeck measurements). Another possibility is that because the free carrier concentration is low (inferred from the electric resistance) the silver paste contacts used in the PPMS measurements cause a depletion zone for the samples, $Rb_8Ga_8Si_{38}$ and $Cs_8Ga_8Si_{38}$, which converts these materials from n- to p-type. Further in-depth studies are needed to address this issue.

Table 3. Band Gap Values from Figure 10

parameter	comments			
compound	$Cs_8Ga_8Si_{38}$	$Rb_8Ga_8Si_{38}$	$K_8Ga_8Si_{38}$	$K_8Al_8Si_{38}$
band gap (eV)	1.14	1.18	1.18	1.40

4. CONCLUSION

A series of Si-based clathrates, $A_8Ga_8Si_{38}$ (A = K, Rb, Cs) and $K_8Al_8Si_{38}$, were synthesized. $Cs_8Ga_8Si_{38}$ was synthesized for the first time, and its structure was reported. The type I clathrate structure was confirmed through laboratory powder X-ray diffraction, as well as synchrotron powder X-ray diffraction. Structural details, in particular the gallium occupancies and guest atom anisotropic vibrations, were studied through single crystal X-ray diffraction. The powder samples were sintered by means of SPS, and the phase information and chemical composition were confirmed though electron microprobe analysis. Thermoelectric properties of the sintered pellets were investigated. $K_8Ga_8Si_{38}$ showed the lowest thermal conductivity, whereas $K_8Al_8Si_{38}$ showed the most promising Seebeck coefficient and lowest electrical resistivity at room temperature. The samples were shown to be semiconductors with moderate band gaps determined by SPV spectroscopy. With further optimization, the K-containing clathrates might provide a promising zT at high temperatures.

■ ASSOCIATED CONTENT

Supporting Information

The electron microprobe results on sintered pellets of $K_8Al_8Si_{38}$ and $A_8Tr_8Si_{38}$ (A = K, Rb, Cs) showing the BSE (Back Scattering Electron), A, Al or Ga, and Si element mapping and CIF's for $A_8Ga_8Si_{38}$ (A = K, Rb, Cs). This material is available free of charge via the Internet at http://pubs.acs.org.

■ AUTHOR INFORMATION

Corresponding Author

*E-mail: smkauzlarich@ucdavis.edu.

Notes

The authors declare no competing financial interest.

■ ACKNOWLEDGMENTS

We thank G. Galli and Y. He for useful discussion. F.S. and S.M.K. acknowledge NSF grants DMR-1100313 and DMR-1405973. Work at the University of Delaware was done under the auspices of US DOE-Basic Energy Sciences (DE-SC0008885).

■ REFERENCES

(1) Slack, G. A. *CRC Handbook of Thermoelectrics*; Rowe, D. M., Ed.; CRC Press: Boca Raton, FL, 1995.
(2) Kasper, J. S.; Hagenmul, P.; Pouchard, M.; Cros, C. *Science* **1965**, *150*, 1713.
(3) Nolas, G. S. *The Physics and Chemistry of Inorganic Clathrates*; Springer: Philadelphia, New York, 2014.
(4) Cohn, J. L.; Nolas, G. S.; Fessatidis, V.; Metcalf, T. H.; Slack, G. A. *Phys. Rev. Lett.* **1999**, *82*, 779−782.
(5) Christensen, M.; Johnsen, S.; Iversen, B. B. *Dalton Trans.* **2010**, *39*, 978−92.
(6) Fulmer, J.; Lebedev, O. I.; Roddatis, V. V.; Kaseman, D. C.; Sen, S.; Dolyniuk, J.-A.; Lee, K.; Olenev, A. V.; Kovnir, K. *J. Am. Chem. Soc.* **2013**, *135*, 12313−12323.
(7) Shevelkov, A. V.; Kovnir, K. Zintl Clathrates. In *Zintl Phases: Principles and Recent Developments*; Fassler, T. F., Ed.; 2011; Vol. *139*, pp 97−142.
(8) Condron, C. L.; Kauzlarich, S. M. *Inorg. Chem.* **2007**, *46*, 2556−2562.
(9) He, Y.; Sui, F.; Kauzlarich, S. M.; Galli, G. *Energy Environ. Sci.* **2014**, *7*, 2598−2602.
(10) Baranowski, L. L.; Krishna, L.; Martinez, A. D.; Raharjo, T.; Stevanovic, V.; Tamboli, A. C.; Toberer, E. S. *J. Mater. Chem. C* **2014**, *2*, 3231−3237.
(11) Slack, G. A.; Hussain, M. A. *J. Appl. Phys.* **1991**, *70*, 2694−2718.
(12) Tani, J.; Kido, H. *Phys. B: Condens. Matter* **2005**, *364*, 218−224.
(13) Dresselhaus, M. S.; Chen, G.; Tang, M. Y.; Yang, R.; Lee, H.; Wang, D.; Ren, Z.; Fleurial, J.-P.; Gogna, P. *Adv. Mater.* **2007**, *19*, 1043−1053.
(14) Yi, T.; Chen, S.; Li, S.; Yang, H.; Bux, S.; Bian, Z.; Katcho, N. A.; Shakouri, A.; Mingo, N.; Fleurial, J.-P.; Browning, N. D.; Kauzlarich, S. M. *J. Mater. Chem.* **2012**, *22*, 24805−24813.
(15) Vineis, C. J.; Shakouri, A.; Majumdar, A.; Kanatzidis, M. G. *Adv. Mater.* **2010**, *22*, 3970−3980.
(16) Snyder, G. J.; Toberer, E. S. *Nat. Mater.* **2008**, *7*, 105−114.
(17) Condron, C. L.; Kauzlarich, S. M.; Gascoin, F.; Snyder, G. J. *Chem. Mater.* **2006**, *18*, 4939−4945.
(18) Condron, C. L.; Martin, J.; Nolas, G. S.; Piccoli, P. M. B.; Schultz, A. J.; Kauzlarich, S. M. *Inorg. Chem.* **2006**, *45*, 9381−6.
(19) Anno, H.; Hokazono, M.; Shirataki, R.; Nagami, Y. *J. Mater. Sci.* **2013**, *48*, 2846−2854.

DOI: 10.1021/cm504436v
Chem. Mater. 2015, 27, 2812−2820

(20) Roudebush, J. H.; de la Cruz, C.; Chakoumakos, B. C.; Kauzlarich, S. M. *Inorg. Chem.* **2012**, *51*, 1805−1812.
(21) Tsujii, N.; Roudebush, J. H.; Zevalkink, A.; Cox-Uvarov, C. A.; Snyder, G. J.; Kauzlarich, S. M. *J. Solid State Chem.* **2011**, *184*, 1293−1303.
(22) Mugit, N.; Nakakohara, Y.; Teranishi, R.; Munetoh, S. *J. Mater. Res.* **2011**, *26*, 1857−1860.
(23) Kauzlarich, S. M.; Sui, F. Light Element Group 13-14 Clathrate Phases. In *The Physics and Chemistry of Inorganic Clathrates*; Nolas, G. S., Ed.; Springer: Philadelphia, New York, 2014; Vol. *199*, pp 227−248.
(24) Kroner, R.; Peters, K.; von Schnering, H. G.; Nesper, R. *Z. Kristallogr. - New Cryst. Struct.* **1998**, *213*, 667−668.
(25) Imai, M.; Sato, A.; Udono, H.; Imai, Y.; Tajima, H. *Dalton Trans.* **2011**, *40*, 4045−7.
(26) Nakamura, K.; Yamada, S.; Ohnuma, T. *Mater. Trans., JIM* **2013**, *54*, 276−285.
(27) Hayashi, M.; Kishimoto, K.; Akai, K.; Asada, H.; Kishio, K.; Koyanagi, T. *J. Phys. D: Appl. Phys.* **2012**, 45.
(28) Hayashi, M.; Kishimoto, K.; Kishio, K.; Akai, K.; Asada, H.; Koyanagi, T. *Dalton Trans.* **2010**, *39*, 1113−1117.
(29) von Schnering, H. G.; Kroner, R.; Menke, H.; Peters, K.; Nesper, R. *Z. Kristallogr. - New Cryst. Struct.* **1998**, *213*, 677−678.
(30) He, Y.; Galli, G. *Nano Lett.* **2014**, *14*, 2920−2925.
(31) Baran, V.; Senyshyn, A.; Karttunen, A. J.; Fischer, A.; Scherer, W.; Raudaschl-Sieber, G.; Fässler, T. F. *Chem.—Eur. J.* **2014**, 20.
(32) Rodríguez-Carvajal, J. *Phys. B: Condens. Matter* **1993**, *192*, 55−69.
(33) Blake, N. P.; Mo/llnitz, L.; Kresse, G.; Metiu, H. *J. Chem. Phys.* **1999**, *111*, 3133−3144.
(34) Christensen, M.; Iversen, B. B. *Chem. Mater.* **2007**, *19*, 4896−4905.
(35) Cordero, B.; Gomez, V.; Platero-Prats, A. E.; Reves, M.; Echeverria, J.; Cremades, E.; Barragan, F.; Alvarez, S. *Dalton Trans.* **2008**, 2832−2838.
(36) Condron, C. L.; Martin, J.; Nolas, G. S.; Piccoli, P. M. B.; Schultz, A. J.; Kauzlarich, S. M. *Inorg. Chem.* **2006**, *45*, 9381−9386.
(37) Bentien, A.; Nishibori, E.; Paschen, S.; Iversen, B. B. *Phys. Rev. B* **2005**, *71*, 144107.
(38) Nolas, G. S.; Vanderveer, D. G.; Wilkinson, A. P.; Cohn, J. L. *J. Appl. Phys.* **2002**, *91*, 8970−8973.
(39) Saramat, A.; Svensson, G.; Palmqvist, A. E. C.; Stiewe, C.; Mueller, E.; Platzek, D.; Williams, S. G. K.; Rowe, D. M.; Bryan, J. D.; Stucky, G. D. *J. Appl. Phys.* **2006**, 99.
(40) Christensen, M.; Lock, N.; Overgaard, J.; Iversen, B. B. *J. Am. Chem. Soc.* **2006**, *128*, 15657−15665.
(41) Toberer, E. S.; Christensen, M.; Iversen, B. B.; Snyder, G. J. *Phys. Rev. B* **2008**, 77.
(42) Kuznetsov, V. L.; Kuznetsova, L. A.; Kaliazin, A. E.; Rowe, D. M. *J. Appl. Phys.* **2000**, *87*, 7871−7875.
(43) Dolyniuk, J.-A.; Kaseman, D. C.; Sen, S.; Zhao, J.; Osterloh, F. E.; Kovnir, K. *Chem.—Eur. J.* **2014**, *20*, 10829−10837.
(44) Frame, F. A.; Townsend, T. K.; Chamousis, R. L.; Sabio, E. M.; Dittrich, T.; Browning, N. D.; Osterloh, F. E. *J. Am. Chem. Soc.* **2011**, *133*, 7264−7267.
(45) Gross, D.; Mora-Seró, I.; Dittrich, T.; Belaidi, A.; Mauser, C.; Houtepen, A. J.; Como, E. D.; Rogach, A. L.; Feldmann, J. *J. Am. Chem. Soc.* **2010**, *132*, 5981−5983.
(46) Kronik, L.; Shapira, Y. *Surf. Sci. Rep.* **1999**, *37*, 1−206.
(47) Kronik, L.; Shapira, Y. *Surf. Interface Anal.* **2001**, *31*, 954−965.
(48) Muthuswamy, E.; Zhao, J.; Tabatabaei, K.; Amador, M. M.; Holmes, M. A.; Osterloh, F. E.; Kauzlarich, S. M. *Chem. Mater.* **2014**, *26*, 2138−2146.
(49) Osterloh, F. E.; Holmes, M. A.; Chang, L.; Moulé, A. J.; Zhao, J. *J. Phys. Chem. C* **2013**, *117*, 26905−26913.
(50) Wang, J.; Osterloh, F. E. *J. Mater. Chem. A* **2014**, *2*, 9405−9411.
(51) Zhao, J.; Osterloh, F. E. *J. Phys. Chem. Lett.* **2014**, *5*, 782−786.

DOI: 10.1021/cm504436v
Chem. Mater. 2015, 27, 2812−2820